INSTITUTE OF PHYSICS PUBLISHING JOURNAL OF PHYSICS: CONDENSED MATTER

J. Phys.: Condens. Matter **16** (2004) S1921–S1930 PII: S0953-8984(04)71046-2

Colloidal discs in nematic liquid crystals

N M Silvestre[1], P Patrício[1,2], M Tasinkevych[1], D Andrienko[3] and M M Telo da Gama[1]

[1] Departamento de Física da Faculdade de Ciências and Centro de Física Teórica e Computacional, Universidade de Lisboa, Avenida Professor Gama Pinto 2, P-1649-003 Lisboa Codex, Portugal
[2] Instituto Superior de Engenharia de Lisboa, Rua Conselheiro Emídio Navarro 1, P-1949-014 Lisboa, Portugal
[3] Max Planck Institute for Polymer Research, Ackermannweg 10, 55128 Mainz, Germany

Received 27 October 2003
Published 30 April 2004
Online at stacks.iop.org/JPhysCM/16/S1921
DOI: 10.1088/0953-8984/16/19/005

Abstract

We use adaptive finite elements methods to investigate a variety of structures in inverted nematic emulsions numerically. In particular, we study dipolar and quadrupolar interactions between colloidal discs in two-dimensional nematics. The behaviour of colloidal particles near a substrate and at a nematic–isotropic interface are also considered.

(Some figures in this article are in colour only in the electronic version)

1. Introduction

The discovery of novel mechanisms of colloidal interactions [11] increases the range of soft matter structures that may be used in applications. Inverted nematic emulsions (NE) have been the subject of numerous studies in recent years. Although most of this work considers three-dimensional systems, two-dimensional (2D) films have also been studied theoretically [9, 10, 15] and experimentally [1]. Except for the linear regime, where analytical solutions are known, the study of colloidal interactions in NE requires the use of sophisticated numerical methods.

In this paper, we review some of our results on 2D NE. To set the notation we review the elastic theories of Frank and Landau–de Gennes (LdG) in section 2. In general, the non-linearities present in the theories prevent analytical solutions. We developed a numerical scheme, based on finite elements methods, to minimize an arbitrary functional and have used it [9] to study the dipolar interaction between two colloidal discs (see section 4). It was shown that the energy of the quadrupolar configuration for a single disc is always lower than that of the dipolar configuration in 2D [15] and that the interaction of two colloidal discs exhibits interesting non-linear effects (see section 6). More recently we studied the behaviour of a colloidal disc near a planar substrate (section 7) and close to a nematic–isotropic (NI) interface (section 8).

2. Elastic free energy

In the nematic phase the molecules exhibit a local average orientation $\mathbf{n}(\mathbf{r})$, referred to as the director field. $\mathbf{n}$ is unitary and $\mathbf{r} = (x, y, z)$ in 3D. Considering small variations of $\mathbf{n}$ the free-energy density can be expanded up to second order in $\nabla_i \mathbf{n}_j$. The free energy is invariant under uniform rotations of the whole system and under the symmetry operations $\mathbf{n} \to -\mathbf{n}$ and $\mathbf{r} \to -\mathbf{r}$. The elastic free energy of the nematic phase can then be written as the sum of the contributions due to three types of distortions: *splay*, *twist* and *bend*, and we obtain the Frank free energy [5]:

$$F_{\mathbf{n}} = \tfrac{1}{2} \int_{\Omega} \mathrm{d}^3 r \, \{K_{\mathrm{splay}}(\nabla \cdot \mathbf{n})^2 + K_{\mathrm{twist}}[\mathbf{n} \cdot (\nabla \times \mathbf{n})]^2 + K_{\mathrm{bend}}[\mathbf{n} \times (\nabla \times \mathbf{n})]^2\}. \tag{1}$$

Ω is the volume of the three-dimensional sample. When the nematic is confined to 2D the second term is zero and there are splay and bend distortions only. We can write the director as a function of the tilt angle $\theta(\mathbf{r})$, $\mathbf{n}(\mathbf{r}) = (\cos\theta(\mathbf{r}), \sin\theta(\mathbf{r}))$, and using the one constant approximation, $K_{\mathrm{splay}} = K_{\mathrm{bend}} = K$, equation (1) becomes

$$F_{\mathbf{n}} = \frac{K}{2} \int_{\Sigma} \mathrm{d}^2 r \, [(\nabla \cdot \mathbf{n})^2 + (\nabla \times \mathbf{n})^2] \tag{2}$$

$$= \frac{K}{2} \int_{\Sigma} \mathrm{d}^2 r \, (\nabla\theta)^2. \tag{3}$$

Σ is the area of the two-dimensional film. Note that equation (3) is similar to the elastic free energy of the two-dimensional XY model [10]. The director field is singular in the presence of topological defects and thus the Frank free energy is defined only outside of the defect core.

Within this formalism it is possible to define a surface free energy, usually of the Rapini–Papoular form, to take into account the interaction of the nematic with a surface [14]:

$$F_{\mathbf{n},\mathrm{surface}} = \int_{\partial\Sigma} \mathrm{d}r \, \frac{W}{2}[1 - (\mathbf{n} \cdot \boldsymbol{\nu})^2]. \tag{4}$$

$\boldsymbol{\nu}$ denotes the preferred orientation of the nematic at the surface while W is the coupling constant. For a colloidal particle of radius a, the ratio aW/K determines the existence of topological defects.

Divergences may be avoided if one describes the system by a Landau free-energy density $f_{\mathbf{Q}}$, which is a function of the temperature, volume, the local tensor order parameter, and its spatial derivatives [17]:

$$f_{\mathbf{Q}} = -\frac{A(T)}{2}\mathrm{Tr}\{\mathbf{Q}^2\} + \frac{B}{3}\mathrm{Tr}\{\mathbf{Q}^3\} + \frac{C}{4}\mathrm{Tr}\{\mathbf{Q}^2\}^2 + \frac{L_1}{2}\partial_\gamma Q_{\alpha\beta}\partial_\gamma Q_{\beta\alpha} + \frac{L_2}{2}\partial_\beta Q_{\alpha\beta}\partial_\gamma Q_{\gamma\alpha}. \tag{5}$$

Here summation over repeated indices is implied and Tr denotes the trace operation. The first three terms describe the bulk free energy while the last two describe elastic distortions. For a uniaxial nematic one can construct a traceless tensor order parameter [2] which we write as $Q_{\alpha\beta}(\mathbf{r}) = S(\mathbf{r})(n_\alpha(\mathbf{r})n_\beta(\mathbf{r}) - \delta_{\alpha\beta}/D)$, where D is the dimension of the sample and $S(\mathbf{r}) \leqslant 1$ is the scalar order parameter, that vanishes in the isotropic phase. Close to the nematic–isotropic transition $A(T)$ is a linear function of the temperature, and B and C are constants [8]. Inserting $Q_{\alpha\beta}$ in (5), integrating over the whole sample, and comparing with equation (1) reveals that the Frank free energy is minimised in the limit of constant order parameter $S(\mathbf{r}) = S_{\mathrm{bulk}}$. One also finds that $L_1 = K_{\mathrm{twist}}/(2S_{\mathrm{bulk}}^2)$ and $L_2 = (K_{\mathrm{splay}} - K_{\mathrm{twist}})/(2S_{\mathrm{bulk}}^2) = (K_{\mathrm{bend}} - K_{\mathrm{twist}})/(2S_{\mathrm{bulk}}^2)$ [17].

For a 2D system $\mathrm{Tr}\{\mathbf{Q}^3\}$ vanishes. If we consider the one-constant approximation then $L_2 = 0$ and $L_1 = K/2S_{\mathrm{bulk}}^2$, and the LdG free energy becomes

$$F_{\mathbf{Q}} = \int_{\Sigma} \left(-\frac{A(T)}{2}\mathrm{Tr}\{\mathbf{Q}^2\} + \frac{C}{4}\mathrm{Tr}\{\mathbf{Q}^2\}^2 + \frac{L_1}{2}\partial_\gamma Q_{\alpha\beta}\partial_\gamma Q_{\beta\alpha} \right). \tag{6}$$

Stability requires that the total free energy is bounded from below; consequently, C is positive. The equilibrium orientational order parameter is $S_{\text{bulk}} = \sqrt{2A/C}$. The LdG free energy may be written as a functional of the tilt angle $\theta(\mathbf{r})$ and the orientational order parameter $S(\mathbf{r})$. Within this approach one can estimate the core energy of a defect of charge q to be given by [15]

$$F_{\text{core}} = q^2 \frac{\pi K}{2}. \tag{7}$$

Finally, let us consider the surface free energy within the LdG formalism. Taking $\boldsymbol{\nu}$ as the preferred orientation at the boundary $\partial\Sigma$, we can construct a tensor order parameter $Q^0_{\alpha\beta} = S^0(\nu_\alpha \nu_\beta - \delta_{\alpha\beta}/d)$ and expand the surface free energy around $\mathbf{Q}^0$:

$$F_{\mathbf{Q},\text{surface}} = \int_{\partial\Sigma} \mathrm{d}r \left[\frac{W'}{2} \text{Tr}\{(\mathbf{Q} - \mathbf{Q}^0)^2\} + \text{O}(\text{Tr}\{(\mathbf{Q} - \mathbf{Q}^0)^3\}) \right]. \tag{8}$$

Up to second-order terms we obtain an expression that is effectively the same as (4) with $W = W'S^0$. This free-energy contribution corresponds to the boundary conditions in the strong anchoring regime.

3. Numerical minimization scheme

The director field follows from minimization of the total free energy with the constraint that $\mathbf{n}$ is a unit vector, or that $Q_{\alpha\beta}$ is traceless. Even in the one-constant approximation and under the assumption of strong anchoring, this is a difficult problem to solve due to the additional constraint [14].

We have developed a numerical minimization scheme based on the finite elements method. The 2D geometry is filled with triangles using a triangulation algorithm, respecting the predefined physical boundaries. Standard numerical procedures [12] are used to minimize the free energy with respect to any function, e.g. the tilt angle $\theta(\mathbf{r})$ or the tensor order parameter $Q_{\alpha\beta}$. This function is then known at the vertices of the mesh and is linearly interpolated within each triangle.

Adapted meshes may be generated if the Hessian of the solution is known. Notice that the number of triangles does not need to be conserved. Over the regions where the Hessian is small the elements are large, while over the regions where the Hessian is large the triangles are several orders of magnitude smaller. In the numerical discretization, the functions are linearly interpolated within each triangle and their second derivatives are not defined there. Thus the Hessian at vertex k, $\mathcal{H}^k_{\alpha\beta}$, is estimated using the following 'weak' definition (see [4], p 349):

$$\mathcal{H}^k_{\alpha\beta} = -\frac{\int (\partial\Phi/\partial x_\alpha)(\partial v^k/\partial x_\beta)\,\mathrm{d}S}{\int v^k\,\mathrm{d}S}, \tag{9}$$

where Φ is the function that we want to determine. v^k is the piecewise linear hat function associated with vertex k ($v^k = 1$ at vertex k, $v^k = 0$ at all other vertices and $v^k(x, y)$ is linearly interpolated within each triangle), $x_1 = x$ and $x_2 = y$. To construct a new anisotropic non-uniform mesh we associate a metric to each vertex of the old mesh, i.e. a two-dimensional matrix that defines the new triangle size near that vertex. The size of the new triangle is chosen to guarantee that the difference between the interpolated function $\Phi(x, y)$ and the exact solution is equally distributed over the new mesh.

The required map, $\mathcal{M}^k_{\alpha\beta}$, at vertex k, is a two-dimensional positive-definite matrix that may be defined as the *absolute value* of the Hessian $\mathcal{H}^k$:

$$\mathcal{M}^k = c_0 \mathcal{O} \begin{pmatrix} |\lambda_1| & 0 \\ 0 & |\lambda_2| \end{pmatrix} \mathcal{O}^{-1}, \tag{10}$$

where $\mathcal{O}$ is the orthogonal matrix that diagonalizes the Hessian, and λ_1 and λ_2 the corresponding eigenvalues. The constant c_0 controls the number of mesh triangles. To avoid problems due to the divergence of the Hessian, the eigenvalues are bounded by

$$\lambda_\alpha = \min\left(\max\left(|\lambda_\alpha|, \frac{1}{c_0 h_{\max}^2}\right), \frac{1}{c_0 h_{\min}^2}\right), \tag{11}$$

where $h_{\max}$ and $h_{\min}$ are the minimal and maximal mesh edge lengths. We used the 2D mesh generator [4] (*BL2D* package). The construction of the new adapted mesh, given the old one and the metric map, is automatically generated by a *BL2D* subroutine. Starting from a mesh with 656 points and ending with 21 888 points, we obtain results with an accuracy of 10^{-4}; the calculation takes about 80 min on a Digital Alpha station at 600 MHz.

4. Dipolar interaction in 2D nematics

A stringent test of the numerics is provided by considering two circular discs of radius a separated by a distance R along the x-axis, in the one elastic constant approximation, and comparing the numerical results with the analytical results of [10]. Since equation (1) is singular at the defects we pinned $a - 1$ defect near each disc at a distance r_{d_1} measured from the centre the disc. The system exhibits mirror symmetry with respect to the x-axis.

The tilt angle θ is fixed at the physical boundaries. The far-field director $\mathbf{n}_0$ is taken parallel to the x-axis ($\theta = 0$) and homeotropic boundary conditions were imposed at the surfaces of the colloidal discs. On the x-axis, θ is set to zero everywhere except between the discs and at their companion defects. The core energies contribute with a constant and were not taken into account.

As a first test of the numerics, one single disc was considered. The free energy as a function of the defect distance r_d was calculated, for a dipole parallel to the far-field director. The equilibrium free energy was found for a defect at $r_d = (1.41 \pm 0.01)a$, in agreement with the analytical [10] and experimental [1] results.

We used a rectangular integration region of size $L_x \times L_y = 50a \times 20a$ which was sufficiently large to make finite-size effects negligible. With this technique we are able to study defects with cores as small as $10^{-3}a$.

Near the core the elastic distortion is determined by the defect alone. We found that the separation of the discs had no influence on the position of the outer defect. The latter is then pinned at $r_{d_2} = 1.41a$. In this study the lowest elastic free energy was obtained at a disc separation $R = 2.82a$, with an inner defect at $r_{d_1} = 1.41a$.

When considering the equilibrium position of the inner defect r_{d_1}, as a function of the disc separation R, one finds three different regimes [9]. At small disc separation ($R \leqslant 2.82a$) the defect is at the mid-point between the discs, $r_{d_1} = R/2$. In an intermediate regime ($2.82a \leqslant R \leqslant 6.5a$) the defect position varies non-monotonically with R. Finally, at large disc separations the position of the inner defect is independent of R and is given by that of an isolated disc.

The Frank free energy exhibits a pronounced minimum at $R = (2.82 \pm 0.01)a$ (figure 1(a)), comparable to the experimentally obtained value of $(2.6 \pm 0.2)a$ by Cluzeau *et al* [1]. The signature of the dipolar interaction at large disc separations may be seen in figure 1(b). The interaction free energy decays as a power law, R^{-2}.

5. Dipolar versus quadrupolar configurations

Recently Pettey *et al* [10] used the Frank elastic energy (equation (3)), to obtain analytical expressions for the free energy of a disc of radius a, with a dipolar topological defect (see

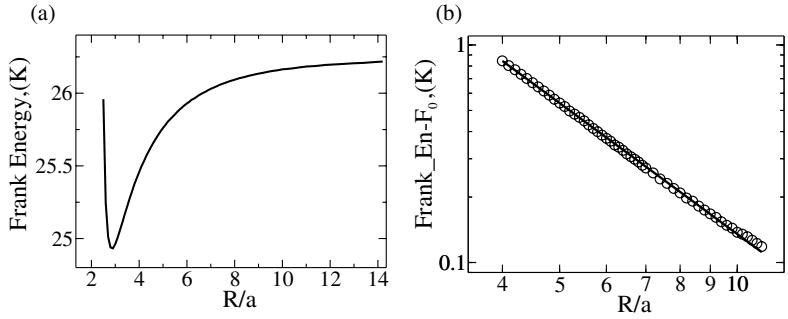

Figure 1. (a) The 2D Frank free energy as a function of the disc separation. The free energy has a pronounced minimum at $R = (2.82 \pm 0.01)a$. (b) Log–log plot of the interaction free energy versus disc separation. F_0 is the free energy at infinite separation. Circles represent the numerical results. The line is proportional to R^{-2}.

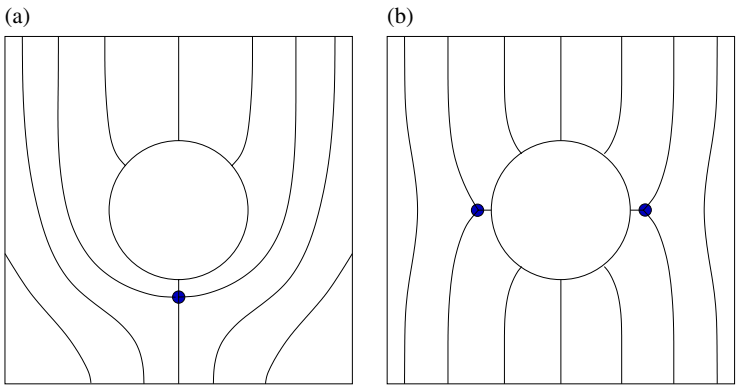

Figure 2. (a) Dipolar configuration. A colloidal particle with radius a is accompanied by a defect with topological charge $q = -1$ located at $r_d = \sqrt{2}a$ from the centre of the particle; (b) quadrupolar configuration. Two defects with topological charge $q = -1/2$ are located at $r_d = \sqrt[4]{7/3}a$ from the centre of the particle.

figure 2(a). The equilibrium defect position was found at $(r_d)_{eq} = \sqrt{2}a$. In a 2D nematic, however, configurations $\mathbf{n}$ and $-\mathbf{n}$ are equivalent allowing a quadrupolar defect configuration, where the disc is accompanied by two $-1/2$ topological defects (figure 2(b)) yielding [15]

$$F_{\text{quadrupolar}} = -\frac{\pi K}{2}\log 2\left(\frac{a^3}{r_d^3} - \frac{a^7}{r_d^7}\right) + \frac{\pi K}{2}\log\frac{a}{\xi_q} + F_{\text{core}}, \tag{12}$$

where $\xi_q = |q|\zeta$ is the core radius, q is the charge of the defect and ζ the nematic correlation length. F_{core} is given by equation (7).

Minimizing (12) with respect to r_d yields $(r_d)_{eq} = \sqrt[4]{7/3}a$, as obtained by Fukuda and Yokoyama [6] using a simple force balance argument.

The difference between the free energy of the dipolar configuration and (12) is a function of the correlation length ζ and the disc's radius [15]:

$$F_{\text{dip}} - F_{\text{quad}} \approx \frac{\pi K}{2}\left(2.08 + \log\frac{a}{\zeta}\right). \tag{13}$$

Since far from the nematic–isotropic transition $a \gg \zeta$, this difference is always positive, and thus the quadrupolar configuration is the most stable within this description.

6. Quadrupolar interaction in 2D nematics

The interaction of two colloidal discs, each with two $-1/2$ topological defects, was considered in [15]. The far field $\mathbf{n}_0$ is along the y-axis. The origin of the reference frame is at the centre of one of the particles; the centre of the second particle is at $\mathbf{R} = (R\cos\alpha, R\sin\alpha)$. If the separation between particles is large, the nematic distortion is approximately given by the sum of the isolated quadrupolar solutions, $\theta \approx \theta_1 + \theta_2$. Assuming homeotropic boundary conditions this yields for the long-range interaction energy

$$F_{\rm int} \approx 6\pi K (r_{\rm d}^4 + a^4) \frac{1 - 2\sin^2 2\alpha}{R^4}. \tag{14}$$

The effective interaction between discs decays as R^{-4} and is strongly anisotropic: repulsive if the particles are aligned horizontally or vertically ($\alpha = 0$ or $\pi/2$, respectively), and attractive at intermediate oblique orientations.

At small disc separations, the nematic deformation is no longer the sum of isolated quadrupolar solutions. In order to study this we have used the numerical scheme described previously. We considered discs, of radius a, in a box of side $20a$. Although analytically simpler, the Frank free energy (1) is plagued with divergences of $\nabla\theta$ at the defects and is not the most adequate for numerical computations, and thus we resorted to the LdG free energy (6).

To test the numerical accuracy of the procedure we calculated the nematic configuration for the isolated disc, and found two half-integer defects at $r_{\rm d} = (1.23 \pm 0.01)a$, in very good agreement with the analytical result.

The effective interaction between discs is plotted in figure 3(a) as a function of the distance R between discs, at different orientations ($\alpha = 0, \pi/4, \pi/2$). The long-range decay R^{-4} is confirmed at large disc separations. However, at smaller separations, the free energy changes dramatically. Orientations that are repulsive at large separations (e.g., $\alpha = 0, \pi/2$) become attractive at different threshold distances ($R_{\rm th} \approx 5a$ and $R_{\rm th} \approx 3a$, respectively). This change in behaviour is accompanied by the displacement of the defects around the discs (see figure 4). In addition, at short distances, the free energy corresponding to the parallel orientation ($\alpha = 0$) decreases below that of the large distance preferred oblique orientation ($\alpha = \pi/4$). At large R the discs prefer an oblique orientation (with $\alpha = \pi/4$), that changes to parallel (with $\alpha = 0$) as their separation decreases [15].

The interaction between discs at small separations was also analysed. For strong homeotropic anchoring, and for all orientations α, we observed a repulsion when the discs are nearly at contact, at $R \approx 2.1a$. We relaxed the strong anchoring condition and calculated the total elastic free energy as a function of the distance R between discs, for three reduced anchoring strengths ($aW/K = 250, 10, 7.5$). The results are plotted in figure 3. These anchorings are strong enough to induce defects in the nematic. A repulsion is obtained at small separations for strong anchoring ($aW/K = 250$) but vanishes at a critical anchoring strength that lies between $7.5 < aW/K < 10$. We predict that below this anchoring strength coalescence of droplets may occur.

7. Key-lock

The interaction of a topological defect with a planar wall was considered by Imura and Okano [7] using the *method of images*. The same method has been used to study the interaction of a colloidal disc with a planar wall, with homeotropic boundary conditions. This is equivalent to the interaction of two colloidal discs in a nematic with a fixed orientation, at the midplane (line) between the colloids. At long distances, one finds that the interaction is given by

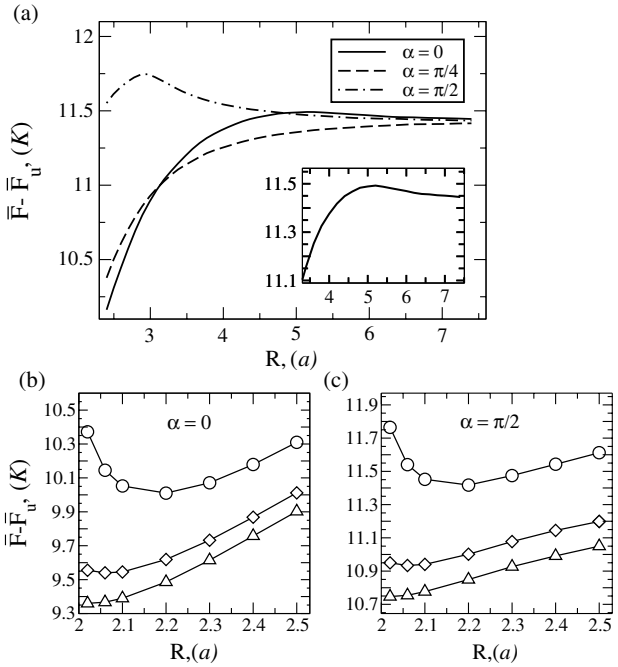

Figure 3. (a) Reduced elastic free energy $\bar{F} = F/K$ as a function of the distance R between discs, at different orientations ($\alpha = 0, \pi/4, \pi/2$). Bottom: reduced elastic free energy $\bar{F} = F/K$ as a function of the discs separation R, for three anchoring strengths, $aW/K = 250, 10, 7.5$, corresponding to the circles, diamonds and triangles, respectively. (b) Parallel alignment ($\alpha = 0$); (c) perpendicular alignment ($\alpha = \pi/2$). $F_{\rm u} = F[S = S_{\rm bulk}]$ is the LdG free energy of a uniform equilibrium nematic.

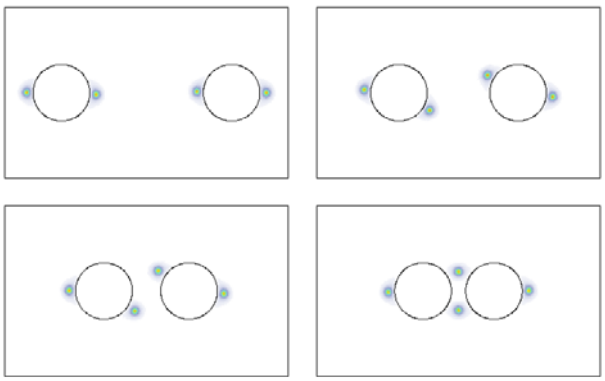

Figure 4. Nematic configurations at several separations for horizontal alignment $\alpha = 0$. The nematic order parameter varies between $S = 0$ (grey regions) and $S = S_{\rm bulk}$ (white).

equation (14) with $R = 2R'$ and $\alpha = \pi/2$. R' is the distance from the centre of the disc to the planar wall. At short distances there is a repulsion (see figure 5).

By adding a cavity to the wall this repulsion may be turned into an attraction [13]. We find that the attraction is stronger for cavities with shapes that are related to that of the disc (see figure 6) and that the minimum free energy occurs when the disc is deep inside the cavity. The colloidal disc plays a role similar to a *key* with the cavity being the *lock*.

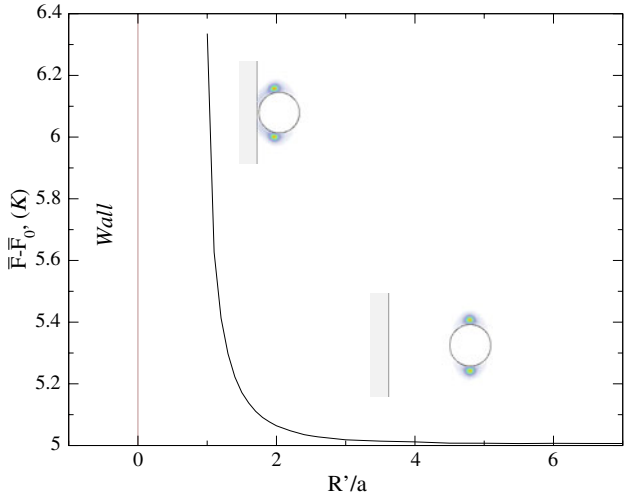

Figure 5. Reduced elastic free energy $\bar{F} = F/K$ as a function of the distance R' of the centre of the disc from the planar wall. As the disc approaches the wall the defects move towards it, increasing the colloid–wall repulsion. F_0 is the LdG free energy for the system without colloid.

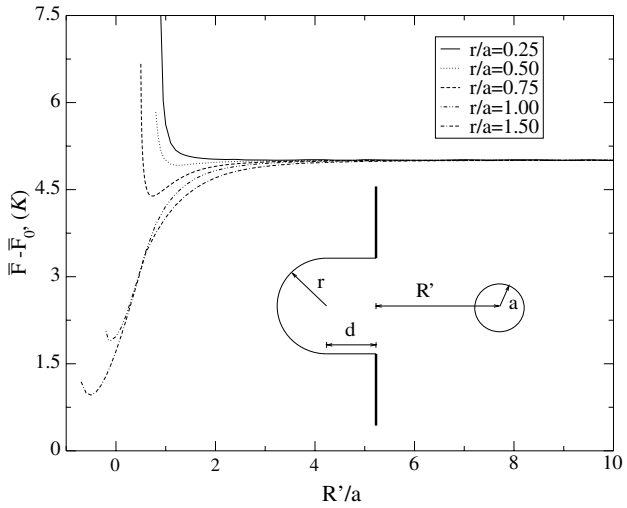

Figure 6. Reduced elastic free energy $\bar{F} = F/K$ as a function of the distance R' of the centre of the disc from the cavity entrance, for $d/a = 0.01$ and different cavity widths ($r/a = 0.25, 0.50, 0.75, 1.00, 1.50$). As r/a approaches unity the interaction energy exhibits a minimum near the cavity.

8. Nematic–isotropic interface

Recently, a drag on colloidal particles by a moving NI interface has been reported [18]. Depending on the cooling rate, West *et al* observed different structures: (a) cellular, with particle-free nematic domains separated by particle-rich regions; (b) striped, with particle-rich regions arranged in stripes; (c) root-like structures.

In order to describe the interaction of a colloid with an NI interface, it is convenient to consider the 3D tensor order parameter formalism, where the cubic term of the bulk energy (5)

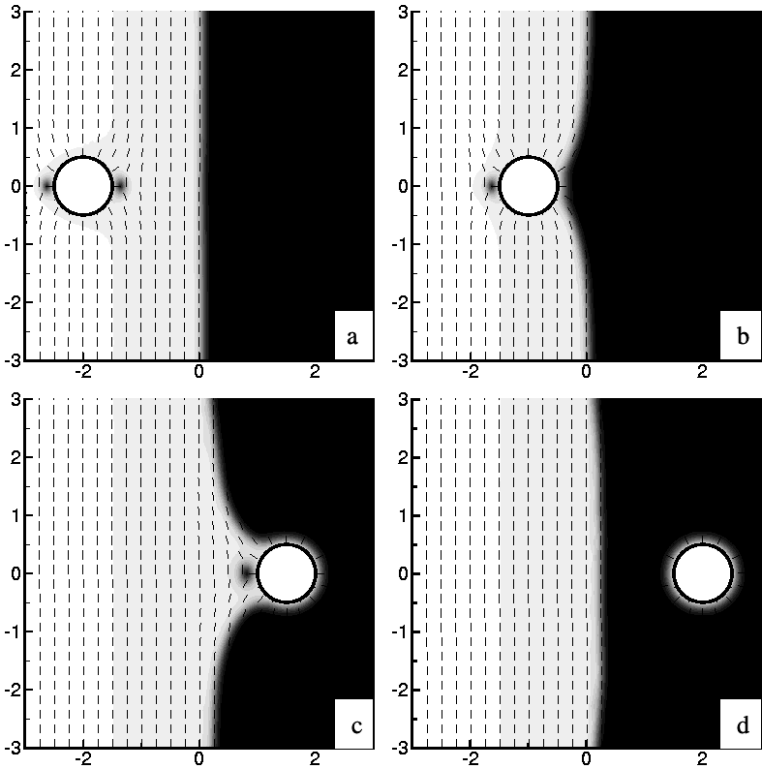

Figure 7. Order parameter and director field for strong homeotropic anchoring at the colloid. The distance of the colloid from the nematic–isotropic interface is (a) $R/2a = -2$; (b) $R/2a = -1$; (c) $R/2a = 1.75$; (d) $R/2a = 2$. The dark region corresponds to $S(\mathbf{r}) = 0$ and the white region to $S(\mathbf{r}) = S_{\text{bulk}}$.

is non-zero, allowing us to treat the first-order NI transition properly. In 3D the interfacial nematic orientation depends on the sign of L_2 [3].

For simplicity, we consider a system with cylindrical symmetry, characterized by inhomogeneities in 2D only, and thus assume that the colloid is a (long) cylindrical particle of radius a, in a 3D nematic [16]. We apply a temperature gradient along the x-axis (by assuming that $A(x)$ varies linearly with x, changing sign at $x = 0$) and set the director at the cold wall ($T < T_{\text{NI}}$) parallel or perpendicular to it, while at the hot wall ($T > T_{\text{NI}}$) the order parameter is set to zero. As a result, a planar nematic–isotropic interface obtains parallel to the yz-plane. The long axis of the cylinder is parallel to the z-axis and the system is translationally invariant in the z-direction. We apply periodic boundary conditions in the y-direction. We assume strong homeotropic anchoring conditions at the particle's surface. In line with the symmetry of the problem we restrict the variations of $\mathbf{n}$ to the xy-plane. We note that in 3D, the presence of spatial non-uniformities may break the continuous rotational symmetry around $\mathbf{n}$ leading to biaxiality. This is described by the full tensor order parameter $Q_{\alpha\beta} = S(\mathbf{r})(n_\alpha n_\beta - \delta_{\alpha\beta}/3) + B(\mathbf{r})(l_\alpha l_\beta - m_\alpha m_\beta)$. The unit vectors $\mathbf{n}$, $\mathbf{l}$, and $\mathbf{m}$ form a local orthonormal triad. If the director is constrained to the xy-plane, $\mathbf{m}$ can be chosen along the z-axis and $\mathbf{l}$ in the xy-plane.

In figure 7 we plot the order parameter and the director field for different positions R of the colloidal particle. As the colloid moves towards the interface, the nematic configurations change in a series of discontinuous transitions, where one or two of the defects are annihilated.

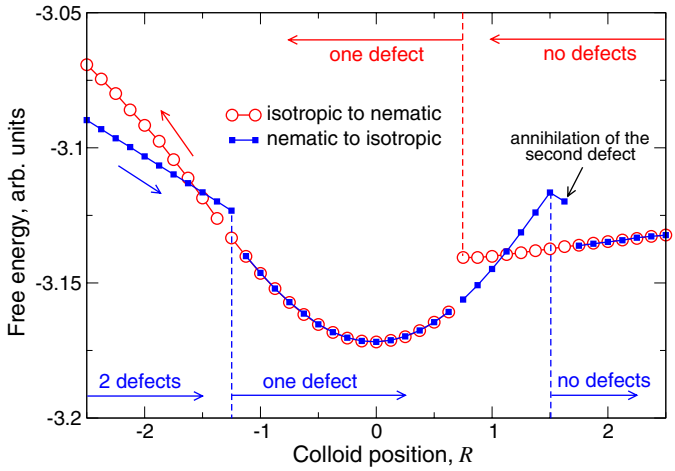

Figure 8. Free energy as a function of the position of the colloidal particle with respect to the nematic–isotropic interface. Strong homeotropic anchoring is imposed at the particle surface. $L_1 = 0.001$ and $L_2 = 0.002$; the temperature gradient is $\partial_x T = 0.025$.

The NI interface bends towards the colloid in order to minimize the elastic free energy. Figure 8 shows the free energy as a function of the position of the colloidal particle. The interaction has a well defined minimum at $R = 0$. In this region the tensor order parameter and the interfacial structures are complex and cannot be described analytically.

9. Conclusions

The numerical method based on adaptive finite-size elements, described above, has proven both accurate and versatile; thus it is a useful tool to solve a wide range of colloidal problems in anisotropic host fluids, including colloids in non-uniform nematics.

References

[1] Cluzeau P, Poulin P, Joly G and Nguyen H T 2001 *Phys. Rev.* E **63** 031702
[2] de Gennes P G and Prost J 1993 *The Physics of Liquid Crystals* 2nd edn (Oxford: Clarendon)
[3] de Gennes P G 1971 *Mol. Cryst. Liq. Cryst.* **12** 193
[4] George P-L and Borouchaki H 1998 *Delaunay Triangulation and Meshing: Application to Finite Elements* (Paris: Hermes)
[5] Frank F C 1958 *Discuss. Faraday Soc.* **25** 19
[6] Fukuda J and Yokoyama H 2001 *Eur. Phys. J.* E **4** 389
[7] Imura H and Okano K 1973 *Phys. Lett.* A **42** 2461
[8] Landau L D and Lifshitz E M 1969 *Statistical Physics* 2nd edn (Oxford: Pergamon)
[9] Patrício P, Tasinkevych M and Telo da Gama M M 2002 *Eur. Phys. J.* E **7** 117
[10] Pettey D, Lubensky T C and Link D R 1998 *Liq. Cryst.* **25** 5
[11] Poulin P, Stark H, Lubensky T C and Weitz D A 1997 *Science* **275** 1770
[12] Press W H, Teukolsky S A, Vetterling W T and Flanery B P 1992 *Numerical Recipes* 2nd edn (Cambridge: Cambridge University Press)
[13] Silvestre N M, Patrício P and Telo da Gama M M 2003 in preparation
[14] Stark H 2001 *Phys. Rep.* **351** 387
[15] Tasinkevych M, Silvestre N M, Patrício P and Telo da Gama M M 2002 *Eur. Phys. J.* E **9** 341
[16] Tasinkevych M, Andrienko D, Patrício P and Telo da Gama M M 2003 in preparation
[17] Vissenberg M C J M, Stallinga S and Vertogen G 1997 *Phys. Rev.* E **55** 4367
[18] West J L, Glushchenko A, Liao G, Reznikov Y, Andrienko D and Allen M 2002 *Phys. Rev.* E **66** 012702